# The Solution Conformation of Hyaluronan: A Combined NMR and Molecular Dynamics Study†

Signe M. A. Holmbeck,‡ Peter A. Petillo,§ and Laura E. Lerner*

*Department of Chemistry, University of Wisconsin, Madison, Wisconsin 53706*

*Received September 7, 1994; Revised Manuscript Received September 15, 1994*⊗

ABSTRACT: Hyaluronan (HA) is a negatively charged glycosaminoglycan that exhibits a wide variety of biological effects mediated by binding to cell-surface and extracellular matrix proteins (hyaladherins). Short HA oligosaccharides have been shown to retain the specific interactions and biological effects of high molecular weight HA. Although it has a simple disaccharide repeating unit, the aqueous solution conformation of HA has been very difficult to determine because of strong coupling and overlapping resonances. In this study, we propose aqueous solution conformations for an octasaccharide of HA, derived from proton−proton NOE data and restrained molecular dynamics. To overcome spectral overlap and strong coupling, alternate methods for extracting distance restraints were employed. Restrained molecular dynamics calculations yielded one set of interglycosidic angle values for the $\beta(1,3)$ linkage ($\phi_{13} = 46°$, $\psi_{13} = 24°$). In contrast, two sets of values for the $\beta(1,4)$ linkage were consistent with the NOE restraints ($\phi_{14} = 24°$, $\psi_{14} = -53°$ or $\phi_{14} = 48°$, $\psi_{14} = 8°$). The potential difference in flexibility for the two linkages is consistent with unrestrained as well as the restrained molecular dynamics trajectories described here. The conformational parameters obtained from restrained molecular dynamics are used to predict helical parameters of high molecular weight HA and will provide a basis for studies of HA binding to proteins.

The glycosaminoglycan hyaluronan (HA)[1] is becoming increasingly important as more biological functions and biomedical applications for it are discovered. HA is a linear polymer composed of the repeating disaccharide unit [(1,3)-*O*-(2-acetamido-2-deoxy-$\beta$-D-glucopyranosyl)-(1,4)-*O*-$\beta$-D-glucopyranuronosyl]$_n$ (Figure 1). Ubiquitous in human tissues, it plays a role in conferring mechanical properties because of its intrinsic viscoelasticity and, in cartilage, because of its interaction with proteoglycans to form aggregates (Toole, 1991). HA is also thought to help control water content and act as a filter for molecules diffusing through the extracellular matrix (Laurent, 1987). However, HA has been shown to have many activities beyond the passive consequences of its physical properties. We list a few of the many available examples here. HA modulates the response of bone marrow to steroids and may be involved in the regulation of hemopoiesis (Siczkowski et al., 1993). Its distribution has been shown to correlate with decidualization and angiogenesis in pregnant mouse uterus (Brown & Papaioannou, 1992). HA can inhibit chondrogenesis (Toole et al., 1972) and also direct the organization of the pericellular matrix of chondrocytes (Knudson, 1993). In addition to cell surface receptors, intracellular binding sites specific for HA have been identified in hepatocytes (Frost et al., 1990).

Many of these activities arise from highly specific interactions with proteins such as the aggrecan core (Christner et al., 1977), versican (Zimmerman & Ruoslahti, 1989; Bignami et al., 1993), hyaluronectin (Bertrand & Delpech, 1985), interleukin 1$\beta$ (Ramsden & Rider, 1992), the $\alpha$3 chain of type VI collagen (Specks et al., 1992), and cell surface receptors such as RHAMM (Hardwick et al., 1992) and CD44 (Toole, 1990). CD44 is a cell adhesion molecule found as a variety of homologues that share some sequence analogy to the HA-binding regions of link protein, aggrecan, and versican (Stamenkovic et al., 1989; Goldstein et al., 1989). Toole (1990) has suggested the name "hyaladherins" for many of these proteins that have homologous HA-binding regions.

In view of the diverse array of proteins that has been shown to bind HA, and the specific nature of these interactions, it is critical to have an accurate picture of the conformation of HA in aqueous solution to aid in modeling. Although HA occurs as a high molecular weight polymer, numerous studies have established that only short oligosaccharides are necessary for recognition and binding by hyaladherins (Toole, 1990). It is interesting to note that a decasaccharide is necessary for binding by aggrecan core and link protein (Hascall & Heinegard, 1974; Christner et al., 1979), while a hexasaccharide is long enough to bind the cell surface HA receptor (Underhill, 1992).

† This work was supported by the Arthritis Foundation and the NIH (R29 AR39801). S.M.A.H. was supported by the Department of Education (P200A10108). The NMR spectrometer used for this work was purchased in part with funds from the NSF (CHE-8813550) and the NIH (STO RRO 4981) shared instrumentation programs.

* Corresponding author.

‡ Current address: The Scripps Research Institute, La Jolla, CA 92037.

§ Current address: Department of Chemistry, University of Illinois, Urbana, IL 61801.

⊗ Abstract published in *Advance ACS Abstracts,* November 1, 1994.

[1] Abbreviations: HA, hyaluronan; NMR, nuclear magnetic resonance; DQF-COSY, double-quantum-filtered correlation spectroscopy; TOCSY, total correlation spectroscopy; HMQC, heteronuclear multiple quantum correlation; HMBC, heteronuclear multiple bond correlation; NOESY, nuclear Overhauser enhancement spectroscopy; J/R, jump−return; HSQC-NOESY, heteronuclear single quantum correlation nuclear Overhauser enhancement spectroscopy; NOE, nuclear Overhauser enhancement; GlcA, $\beta$-D-glucuronate; GlcNAc, *N*-acetylglucosamine or 2-acetamido-2-deoxy-$\beta$-D-glucose.

0006-2960/94/0433-14246$04.50/0 © 1994 American Chemical Society

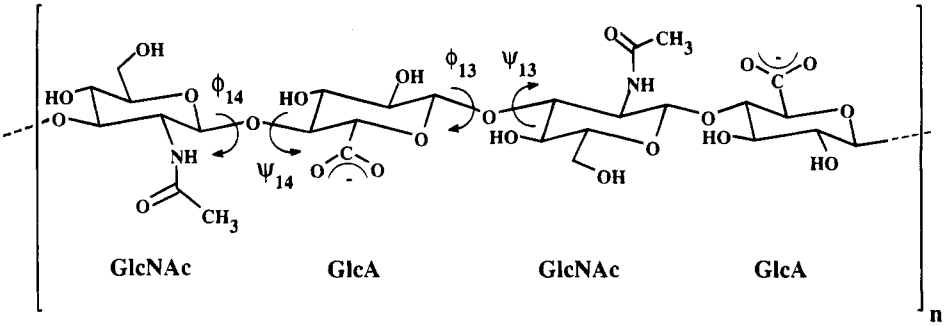


FIGURE 1: Schematic drawing of HA showing $\phi$ and $\psi$ angles as defined in the text.

Although the ability of HA to interact with specific proteins is related to its conformation in aqueous solution, as yet little direct evidence for this conformation has been published. Previously, Scott et al. (1984) used results from X-ray fiber diffraction data and computer calculations in combination with NMR chemical shift and coupling constant data in DMSO to propose a secondary structure for HA in DMSO. The most salient feature of this model is a series of intraring hydrogen bonds, which would inhibit the flexibility of the structure and account for the stiffness observed in rheological studies of the polymer. However, no detailed information about the glycosidic angles was determined. Here we present a $^1$H NMR study of an octasaccharide derived from HA ($HA_4$, where 4 is the number of disaccharide repeating units), using a combination of NOE spectroscopy, coupling constant measurements, and molecular modeling, to determine the most probable conformations about the glycosidic linkages and the most probable orientation of the amide proton (NH) in aqueous solution. We also present the results of molecular dynamics calculations on the two linkages.

## EXPERIMENTAL PROCEDURES

*Materials.* Highly purified high molecular weight (1 000 000−1 800 000) sodium hyaluronate (Hyalumed) was purchased from Genzyme (Boston, MA). Bovine testicular hyaluronidase was from Worthington Biochemical Corporation (Freehold, NJ). Bio-gel P-30 and P-2 polyacrylamide beads were purchased from Bio-Rad Laboratories (Richmond, CA). Deuterium oxide (99.9%) was purchased from Cambridge Isotope Laboratories (Woburn, MA). All $H_2O$ used was filtered through a Milipore Milli-Q water system (Waters Associates, Millford, MA). All other chemicals used were reagent grade.

*Sample Preparation.* The hyaluronan octasaccharide containing four repeating disaccharide units ($HA_4$), with $\beta$-D-glucuronate (GlcA) on the nonreducing end and 2-acetamido-2-deoxy-D-glucose (*N*-acetylglucosamine, GlcNAc) on the reducing end, was prepared by enzymatic degradation of high molecular weight hyaluronan, as described in previous work (Holmbeck & Lerner, 1993).

One sample for NMR was prepared by dissolving 25 mg of $HA_4$ in 700 $\mu$L of 100 mM sodium phosphate (pH 7.2) in 90% $H_2O$/10% $D_2O$. For complete $^1$H and $^{13}$C assignment of the $HA_4$ oligosaccharide, a second sample was prepared by lyophilization of 5 mg of $HA_4$ three times from 99.9% pure $D_2O$. The sample was then diluted to a final volume of 700 $\mu$L by the addition of 99.99% $D_2O$ containing 100 mM sodium phosphate (pH 7.2) (uncorrected for deuterium).

*NMR.* All spectra were obtained on a Varian Unity 500 MHz spectrometer. Proton and carbon-13 assignments of the $HA_4$ at 2 °C were made using DQF-COSY (Piantini et al., 1982), TOCSY (Bax & Davis, 1986), 1D TOCSY (Kessler et al., 1986), HMQC (Bax & Subramanian, 1986), and HMBC (Summers et al., 1986) spectra (available upon request).

NOESY spectra (Macura & Ernst, 1980) were recorded at 2 °C for two reasons. At this temperature, the exchange of amide protons with water is slowed to a point where it does not interfere with NOE build-up significantly, and the water is shifted downfield from the anomeric protons. To suppress the signal from $H_2O$, a jump−return sequence (Plateau & Guéron, 1982) was used in place of the final 90° pulse of the NOESY sequence, and a short (0.5 s), low-power presaturation pulse was used during the recycling delay. The effect of this pulse on amide proton intensity was negligible. A 20 ms homospoil pulse was used during the mixing times, which were 50. 75, 100, 125, and 150 ms. Spectra were recorded with 2048 total points in $t_1$ and 512 total points in $t_2$. The spectral width was 4000 Hz in both dimensions. NOESY spectra were processed using Felix versions 1.1 and 2.05 (Hare Research Inc., Woodinville, WA). The time domain data were multiplied by a 90° shifted squared sine bell and zero-filled to 2048 points. Linear prediction of the first point (Marion & Bax, 1989) was used to help eliminate baseline errors. The interferograms were multiplied by a 90° shifted squared sine bell and zero-filled to 2048 points. A third-order polynomial baseline correction was used in the $\omega_1$ dimension. Cross-peak intensities were determined with the point summation routine supplied with the software. Because the jump−return read pulse in the NOESY does not excite the spectrum evenly, peak volumes were multiplied by $\sin(\pi \times \Delta/2 \times 1591\ \text{Hz})$, where $\Delta$ is the difference in frequency (hertz) of the center of the peak in the $f_2$ dimension from the center of the spectrum (the water peak), and 1591 Hz is the offset where the jump−return sequence gave maximum excitation. Cross-peak volumes from both sides of the diagonal were averaged.

Two-dimensional HSQC-NOESY spectra (Peng & Wagner, 1992) were recorded on $HA_4$ in $D_2O$ with 0 and 125 ms mixing times. The spectra were recorded with 1024 total points in $t_1$ and 280 total points in $t_2$. The spectral width was 2232 Hz for protons and 10 950 Hz for carbon-13. Data were multiplied by a Gaussian function in each dimension before Fourier transformation.

*Calculations and Modeling.* All calculations were performed using the MM3* force field as implemented in Macromodel 3.5 (Mohamadi et al., 1990). The effects of

Table 1: Assignment of $HA_4$ Protons (2 °C in $H_2O$)

| internal GlcA protons | δ (ppm) | internal GlcNAc protons | δ (ppm) | end GlcNAc protons | δ (ppm) |
|---|---|---|---|---|---|
| H1 | 4.48 | H1 | 4.54 | αH1 | 5.16 |
| H2 | 3.35 | H2 | 3.86 | αH2 | 4.05 |
| H3 | 3.59 | H3 | 3.72 | αH3 | 3.91 |
| H4 | 3.73 | H4 | 3.55 | αNH | 8.41 |
| H5 | 3.72 | H5 | 3.50 | βH1 | 4.73 |
| | | H6 | 3.80 | βH2 | 3.83 |
| | | H6″ | 3.93 | βH3 | 3.72 |
| | | NH | 8.22 | βNH | 8.47 |
| | | $CH_3$ | 2.03 | | |

Table 2: Assignment of $HA_4$ Internal Ring Carbons (2 °C in $H_2O$) Referenced to the Internal Acetone Methyl Peak (19.8 ppm)

| internal GlcA carbons | δ (ppm) | internal GlcNAc carbons | δ (ppm) |
|---|---|---|---|
| C1 | 102.6 | C1 | 100.9 |
| C2 | 72.0 | C2 | 53.8 |
| C3 | 73.1 | C3 | 81.9 |
| C4 | 79.4 | C4 | 67.9 |
| C5 | 75.8 | C5 | 74.9 |
| | | C6 | 60.1 |
| | | $CH_3$ | 22.1 |

water were simulated using the GB/SA solvation model (Still et al., 1990). A 6,12 Lennard-Jones potential was used for the hydrogen-bonding potential, as has been shown to be appropriate for glucopyranose rings using the MM3* force field (Hajduk et al., 1993). The charges were the default Macromodel v3.5 values, including those for the carboxylate.

For the $\phi$ and $\psi$ energy maps, the appropriate glycosidic linkage of each HA disaccharide was rotated in 5° increments and minimized while $\phi$ and $\psi$ were held constant. Conformations were minimized to a derivative convergence criterion of 0.01 kcal/Å·mol. All dynamics simulations were performed with a 1.0 or 1.5 fs step size, and coupling between the temperature bath and the molecule was updated every 0.2 ps. Two starting conformations were used for the calculations: one set had all four glycosidic angles set to 0°, and in the other set all glycosidic angles were set to 180°. Calculations were performed at 300, 400, and 500 K. Distance restraints in both the minimization and the dynamics were implemented as flat-bottom energetic restraint wells, with a force constant of 100.0 kJ/Å$^2$ and a ±0.5 Å restraint. This value (0.5 Å) was determined from an estimate of the error. Torsion angle restraints were also implemented as flat-bottom energetic restraint wells with force constants of 1000.0 kJ/mol. Trajectories were calculated for 500 ps, and time points were saved every 0.25 ps throughout the time course. Final optimized glycosidic angles were obtained by following the 500 ps trajectory with 25 ps of simulated annealing, over which time the temperature was ramped down to 0 K. Unrestrained molecular dynamics calculations were performed in the same manner, but without the additional constraints.

## RESULTS

The proton and carbon-13 assignments for the HA octasaccharide, $HA_4$, at pH 7.2 and 2 °C are listed in Tables 1 and 2, respectively. The order of these assignments is consistent with those published recently by Toffanin and coworkers (1993) for the internal GlcA and GlcNAc rings of an HA tetrasaccharide in $D_2O$ at 25 °C.

Table 3: Distances Determined As Described in the Text

| protons | distance (Å) |
|---|---|
| GlcNAc H1/GlcNAc NH | 2.7 |
| GlcA H1/GlcNAc NH | 2.5 |
| GlcA H1/GlcNAc N3 | 2.0 |
| GlcNAc H1/GlcA H4 | 2.1 |

For HA, both GlcA and GlcNAc pyranosyl rings have been determined to be in the $^4C_1$ configuration, with no other ring conformations detectable (Sicińska et al., 1993). Therefore, the overall conformation of HA oligosaccharides will be defined by the torsion angles of the glycosidic linkages and the orientations of the side groups. The four glycosidic angles in HA are defined as $\phi_{13}$ = GlcA H1−GlcA C1−O−GlcNAc C3 and $\psi_{13}$ = GlcA C1−O−GlcNAc C3−GlcNAc H3 for the β(1,3) linkage and $\phi_{14}$ = GlcNAc H1−GlcNAc C1−O−GlcA C4 and $\psi_{14}$ = GlcNAc C1−O−GlcA C4−GlcA H4 for the β(1,4) linkage. These angles are indicated in Figure 1.

Proton NOEs between the GlcA and GlcNAc residues are used to define the geometry about the linkages. Of the two major side groups, the carboxylate on GlcA and the acetamido group on GlcNAc, only the orientation of the latter can be defined by proton NOEs. The NOEs that were used to define the glycosidic angles were those observed between GlcA H1 and GlcNAc H3 and between GlcNAc H1 and GlcA H4. In addition, the NOE observed between GlcA H1 and the amide proton helped define the orientations of both the acetamido group and the β(1,3) linkage. The orientation of the acetamido group was also defined by NOEs between GlcNAc H1 and the amide proton and between GlcNAc H3 and the amide proton. The three-bond scalar coupling constant between GlcA H2 and the amide proton further helped to define the dihedral angle between these two protons.

A NOESY spectrum in $H_2O$ (mixing time = 150 ms) is shown in Figure 2. The amide protons are clearly distinguishable. Figures 3 and 4 show the NOE volume build-up curves for the amide and ring protons, respectively. Interproton distances (Table 3) were derived from the slopes of the NOESY build-up curves using the isolated spin pair approximation (Macura & Ernst, 1980):

$$r_{ij} = r_{std}(\sigma_{std}/\sigma_{ij})^{1/6} \quad (1)$$

where $r_{ij}$ is the distance between two protons, $i$ and $j$, $r_{std}$ is a known distance on the molecule of interest, and the $\sigma$'s are the initial slopes of the NOE build-up curves. The two-spin approximation gives reasonably accurate results when there is little contribution to cross-peak intensity from indirect cross relaxation (Keepers & James, 1984; Clore & Gronenborn, 1989), which applies in this case (see Figures 3 and 4). This approach also assumes that all of the $^1H-^1H$ internuclear vectors have the same correlation time. This is a reasonable assumption for intraring $^1H-^1H$ vectors, based on $^{13}C$ $T_1$'s for HA (Hofmann et al., 1983) and $^{13}C$ $T_1$'s and $^1H-^{13}C$ NOEs for simple hexopyranose rings (Hajduk et al., 1993). Whether this assumption applies to interglycosidic $^1H-^1H$ pairs is not easy to establish. However, several studies published on other disaccharides have concluded that internal motions about the glycosidic linkage are on the same

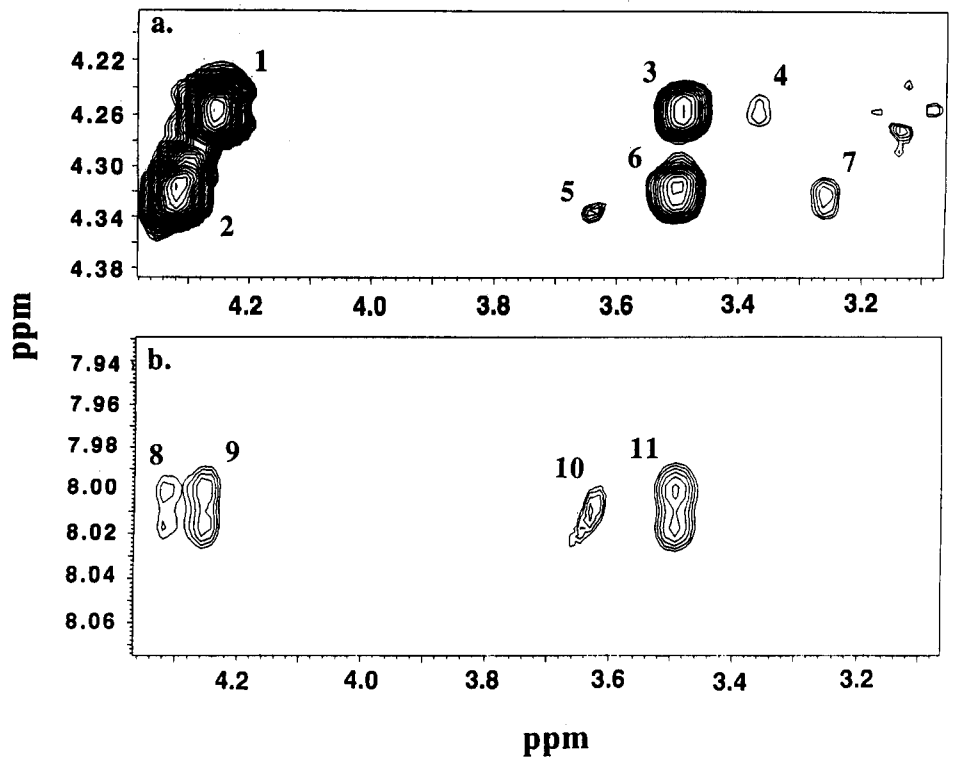


FIGURE 2: NOESY spectrum of $HA_4$ in 90% $H_2O$/10% $D_2O$ at a mixing time of 150 ms, 2 °C. (a) Cross peaks to anomeric protons: (1) GlcA H1 diagonal; (2) GlcNAc H1 diagonal; (3) GlcA H1/GlcNAc H3 and GlcA H5 (overlapped); (4) GlcA H1/GlcA H3; (5) GlcNAc H1/GlcNAc H2; (6) GlcNAc H1/GlcA H4 and GlcNAc H3 (overlapped); (7) GlcNAc H1/GlcNAc H5. (b) Cross peaks to amide protons: (8) NH/GlcNAc H1; (9) NH/GlcA H1; (10) NH/GlcNAc H2; (11) NH/GlcNAc H3, GlcA H4, and/or GlcA H5 (overlapped).

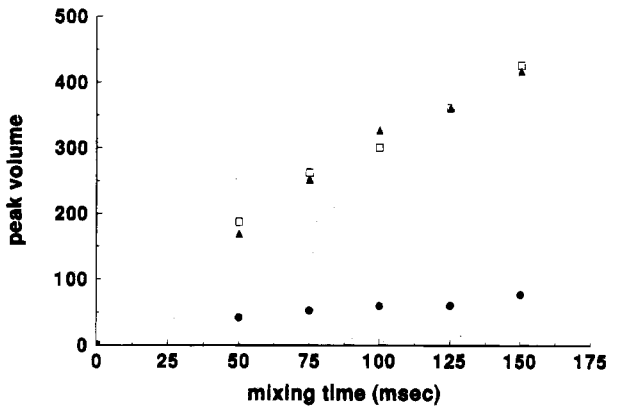


FIGURE 3: NOE build-up curves for the cross peaks in Figure 2a. Peak volume is in arbitrary units. □, GlcA H1/GlcA H3; ▲, GlcNAc H1/GlcA H4 and GlcNAc H3; ●, GlcA H1/GlcNAc H3 and GlcA H5.

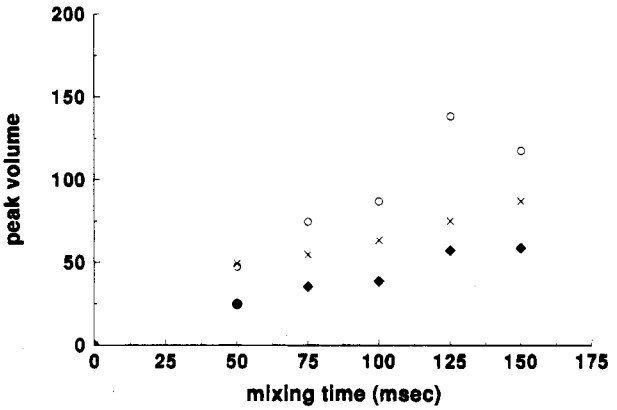


FIGURE 4: NOE build-up curves for the cross peaks in Figure 2b. Peak volume is in arbitrary units. ◆, NH/GlcNAc H3, GlcA H4, and/or GlcA H5; ×, NH/GlcA H1; ○, NH/GlcNAc H1.

time scale as the overall molecular tumbling (Hricovini et al., 1992; Poppe & van Halbeek, 1992; Braccini et al., 1993). Measurements in our laboratory of $^{13}C$ $T_1$'s and $^1H-^{13}C$ NOEs for the 1,3-linked and 1,4-linked HA disaccharides at $^{13}C$ frequencies of 125 and 75 MHz indicated that the rates of any internal motions at the linkage positions were on the order of the overall molecular tumbling rate (P. Hajduk, unpublished results). Therefore, it seems reasonable to assume that a single correlation time can be used to extract interproton distances.

Only internal rings were considered in this analysis. Because the configuration of both rings is known to be $^4C_1$ (Sicińska et al., 1993), the intraring distances can be estimated and the initial slope of their build-up curves can be used as $\sigma_{std}$. Although the GlcA H1/H3, GlcA H2/H4, and GlcNAc H1/H5 intraring NOEs could be integrated, only the GlcA H1/H3 NOE was suitable for use as an internal standard, because H4 and H5 on both rings are strongly coupled ($\Delta\delta \leq J$), which leads to distortions in the NOE (Keeler et al., 1987). The distance between GlcA H1 and H3, $r_{std}$ = 2.6 Å, was taken from X-ray diffraction data on HA (Winter et al., 1975) available from the Brookhaven Protein Data Bank (Abola, et al., 1987; Bernstein et al., 1977).

As for most carbohydrates, the $^1H$ spectrum of HA is plagued by overlapping peaks, and unfortunately the worst overlaps are for exactly those peaks that are important for the determination of conformation. This required special effort to accurately assess the two interglycosidic NOEs between GlcA H1 and GlcNAc H3 and between GlcNAc H1 and GlcA H4. The GlcA H1/GlcNAc H3 cross peak is overlapped with the intraring GlcA H1/GlcA H5 cross peak. Fortunately, the intraring distance between GlcA H1 and

GlcA H5 is relatively fixed (2.4 Å from X-ray diffraction data; Winter et al., 1975), so that $\sigma_{ij}$ for these two protons can be calculated and subtracted from the observed GlcA H1/GlcNAc H3 build-up rate. Since the GlcA H1/H5 distance is comparable to the GlcA H1/H3 distance, it can be seen from Figure 3 that the contribution of an NOE between GlcA H1 and H5 would be small. However, strong coupling between GlcA H5 and H4 complicates the situation. It has been shown (Keeler et al., 1987) that, in an ABX spin system, where A and B are strongly coupled, the initial rate of NOE build-up of A and B from X is

$$(dA/dt)_{t=0} = [(\cos^2\theta)\sigma_{AX} + (\sin^2\theta)\sigma_{BX}]E$$

$$(dB/dt)_{t=0} = [(\cos^2\theta)\sigma_{AX} + (\sin^2\theta)\sigma_{BX}]E \qquad (2)$$

where $\sigma_{AX}$ and $\sigma_{BX}$ are the AX and BX cross-relaxation rates, respectively, and $E$ is the equilibrium magnetization value. The strong coupling parameter, $\theta$, is defined by

$$\tan 2\theta = \frac{J_{AB}}{\delta_A - \delta_B + (J_{AX} - J_{BX})} \qquad (3)$$

Therefore, distortion in an AX NOE from strong coupling in an ABX system can be calculated if the AX and BX distances and the differences between the A and B chemical shifts ($\delta_A - \delta_B$) and coupling constants ($J_{AX} - J_{BX}$) are known, and if a correlation time is assumed. In this case, the ABX system is GlcA H5/H4/H1, and we want to calculate the distortion in the H5/H1 NOE due to the H5/H4 coupling. The H5/H4 coupling constant, $J_{AB}$, has previously been determined to be 9.8 Hz in the $\beta(1,3)$ dimer [GlcA-$\beta$(1,3)-GlcNAc] at 0 °C (Sicińska et al., 1993), and $J_{AX}$ and $J_{BX}$ are virtually zero. Using these values for coupling constants, distances from X-ray diffraction of dried HA fibers, and eqs 2 and 3, we calculate that the measured GlcA H1/H5 build-up rate is about 28% less than it would have been in the absence of strong coupling between H5 and H4. This was taken into account when the GlcA H1/H5 build-up rate was subtracted from the GlcA H1/GlcNAc H3 build-up rate.

Quantification of the other trans-glycosidic NOE between GlcNAc H1 and GlcA H4 also suffers from overlap and strong coupling. The contribution from the overlapping GlcNAc H1/H3 cross peak was calculated and removed. However, the overlap and strong coupling between GlcA H4 and H5 were more difficult to deal with because the GlcNAc H1 potentially could have an NOE to either or both of the GlcA H4 and H5 protons. Structures consistent with the measured NOE build-up rate were back-calculated including the effect of strong coupling. Using Macromodel, the $\phi_{14}$ and $\psi_{14}$ dihedral angles of the $\beta(1,4)$ dimer were rotated in 20° increments, and the GlcNAc H1/GlcA H4, GlcNAc H1/GlcA H5, and GlcNAc H1/GlcA H3 distances for each set of dihedral angles were determined. The GlcNAc H1/GlcA H4 and GlcNAc H1/GlcA H5 distances were used to calculate cross-relaxation rates for each possible distance. These cross-relaxation rates were then summed and normalized to the GlcA H1/H3 standard. Structures were considered plausible if the calculated normalized cross-relaxation rate was within 50% of the measured rate. In Figure 5, $\phi_{14}$ and $\psi_{14}$ angles of these allowed structures are plotted on the energy map for the $\beta(1,4)$ dimer. Allowed structures

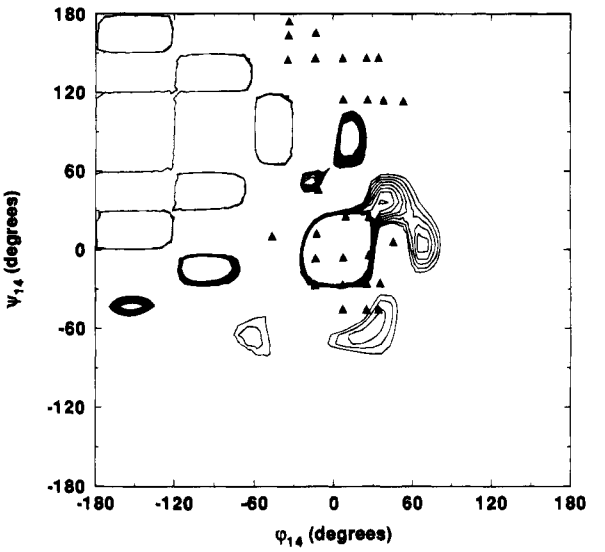


FIGURE 5: Energy contour plot for $\phi_{14}$ and $\psi_{14}$ glycosidic angles for HA disaccharide GlcNAc-$\beta$(1,4)-GlcA. Contour lines represent a 3 kcal/mol increment in energy. $\phi_{14}$ and $\psi_{14}$ pairs for structures found to be consistent with the observed GlcNAc H1/GlcA H4/H5 NOE build-up are indicated with solid triangles.

fall into two groups: one centered around $\phi_{14} = 0°$ and $\psi_{14} = -10°$, where GlcA H4 is close to GlcNAc H1, and another group centered around $\phi_{14} = 0°$ and $\psi_{14} = 150°$, where GlcA H5 is close to GlcNAc H1. This latter group of structures could be eliminated by consideration of an HSQC-NOESY spectrum, Figure 6, which shows a strong NOE between GlcA H4 and GlcNAc H1, but no detectable NOE between GlcA H5 and GlcNAc H1. Therefore, distance constraints were obtained from the maximum and minimum GlcNAc H1/GlcA H4 distances extracted from structures in the first group. The first group also corresponds to structures with energies approximately 10−20 kJ/mol lower than those of the second group.

The NOE cross peak between the amide resonance and resonances at 3.67 ppm could arise from any or all of the overlapped GlcNAc H3, GlcA H4, or GlcA H5 protons. The amide proton three-bond coupling constant for internal GlcNAc residues, $J_{H2-C2-N-H}$, was 9.6 Hz at pH 7, 27 °C. This value is the same as the value measured by Cowman and co-workers (1984) for the HA octasaccharide in aqueous solution at pH 5.5, 25 °C, and by Livant et al. (1992) for the HA tetrasaccharide in aqueous solution at pH 3.27. There is no definitive Karplus relation available relating the H2−C2−N−H dihedral angle to $J_{H2-C2-N-H}$ in N-acetylated amino sugars, so researchers have used Karplus equations derived for model peptides. Depending on the equation used, a $J_{H2-C2-N-H}$ value of 9.6 Hz could indicate all trans (Ramachandran et al., 1971; DeMarco et al., 1978) or a significant fraction of cis conformer (Bystrov et al., 1973). Our NMR-derived distance constraints were consistent with an H2−C2−N−H dihedral angle of 180° ± 50°, and our restrained MD calculations at 300, 400, and 500 K yielded dihedral angles ranging from 169° to 189°, with standard deviations of 14−18°, depending on the temperature (Table 4). Finally, the NH−GlcNAc H1 distance derived from all of the NOE constraints available is 2.7 Å (see Table 3), which is closer to the value expected for an ideal trans conformation (2.9 Å) than an ideal cis conformation (3.8 Å). Note that if the cis conformer predominated, one would

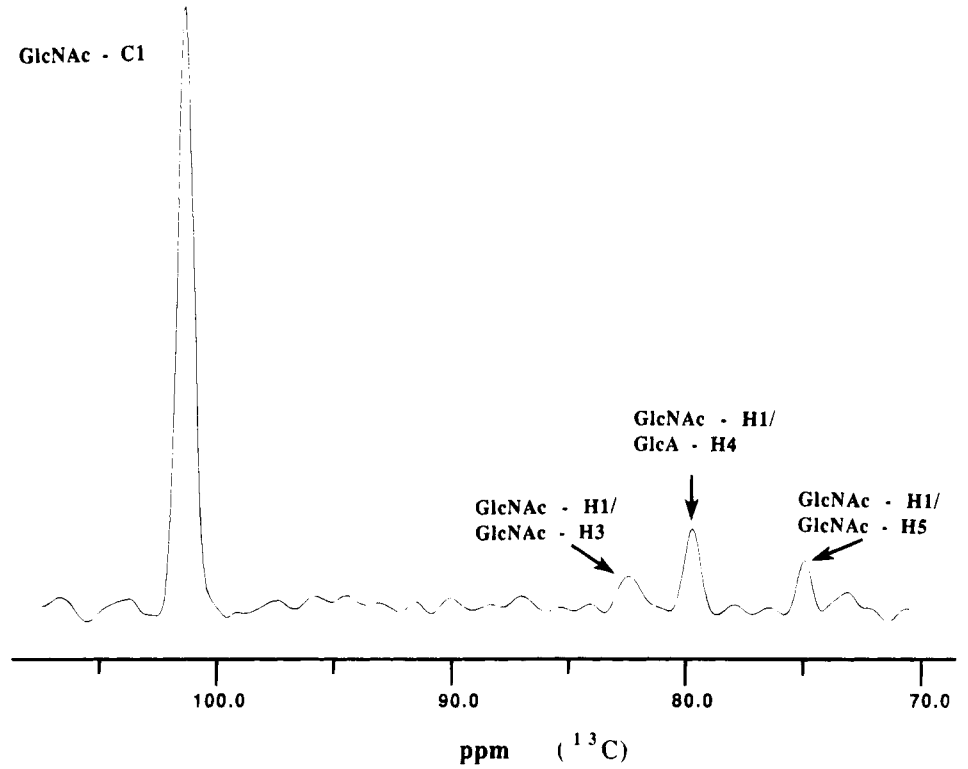


FIGURE 6: Trace through the GlcNAc H1 frequency from the two-dimensional HSQC-NOESY spectrum of $HA_4$. The tallest peak, labeled GlcNAc C1, corresponds to the HSQC cross peak between GlcNAc C1 and GlcNAc H1. The smaller peaks arise from NOEs between GlcNAc H1 and the indicated protons, which appear at the carbon-13 frequency of the carbon directly attached to these protons.

Table 4: Final Optimized Glycosidic Linkage $\phi$, $\psi$, and Amide Dihedral Angles from 500 ps Restrained Molecular Dynamics followed by 25 ps Ramping Down of Temperature and Minimization[a]

| starting structure | temp (K) | $\phi_{13}$ (deg) | $\psi_{13}$ (deg) | $\phi_{14}$ (deg) | $\psi_{14}$ (deg) | amide H2−C2−N−H (deg) |
|---|---|---|---|---|---|---|
| 0° | 300 | 47 | 22 | 23 | −53 | −174 |
| 0° | 400 | 47 | 24 | 26 | −52 | +178 |
| 0° | 500 | 46 | 24 | 24 | −53 | −177 |
| 180° | 300 | 47 | 23 | 48 | 8 | −168 |
| 180° | 400 | 47 | 27 | 47 | 7 | −169 |
| 180° | 500 | 43 | 24 | 24 | −53 | −167 |

[a] In the first column, 0° indicates that all four glycosidic angles were at 0° for the starting structure, and 180° indicates that all four glycosidic angles were 180° in the starting structure.

predict a very intense NH−GlcNAc H2 NOE cross peak and a weak or absent NH−GlcNAc H1 NOE cross peak. In contrast, for pure trans conformer one would predict an NH−GlcNAc H1 NOE cross peak of slightly (~15%) lower intensity than for NH−GlcNAc H2, with both cross peaks significantly less intense than the NH−GlcA H1 cross peak. It can be seen in Figure 2b that the amide NOE cross peaks are most consistent with the trans conformation. All of this evidence taken together suggests that it is reasonable to assume that the predominant conformer is the trans orientation.

When the amide−3.76 ppm NOE build-up rate was calculated using the procedure outlined earlier for the GlcNAc H1/GluA H4 NOE, the GlcNAc H2−C2−N−H amide torsion angle was constrained to 180° ± 20°. It was found that, assuming a 50% error in the NOE, no additional constraints were obtained from this NOE for either the GlcNAc H3/NH or GlcNAc NH/GlcA H4/H5 distances.

Interproton distances are listed in Table 3. The first three distances listed in Table 3 were used to determine the possible $\phi$ and $\psi$ angles for the $\beta(1,3)$ linkage (Figure 7). To do this, the $\phi_{13}$ and $\psi_{13}$ dihedral angles of the $\beta(1,3)$ dimer were each rotated through 360° in 10° increments while the GlcNAc H2−C2−N−H dihedral angle was held at 160°. These rotations were repeated on dimers with the amide dihedral angle held at 170°, 180°, 190°, and 200°. For each structure ($\phi_{13}$, $\psi_{13}$, and amide dihedral angle combination), the GlcA H1/GlcNAc H3, GlcA H1/GlcNAc NH, and GlcNAc NH/GlcNAc H1 distances were measured. Structures were considered possible if these three distances were within ±0.5 Å of the distances listed in Table 3. The $\phi_{13}$ and $\psi_{13}$ dihedral angles of the allowed structures are plotted in Figure 7. The energy contours in Figure 7 were determined in the same manner as those for the $\beta(1,4)$ dimer. No constraints were put on the amide dihedral angle; however, it was in the trans position in the starting structure.

The distances listed in Table 3 were used in restrained molecular dynamics calculations followed by simulated annealing, as described in the Experimental Procedures section, to determine the optimized glycosidic $\phi$, $\psi$, and amide angles (Table 4). Calculations were performed on the GlcA-GlcNAc-GlcA trisaccharide in order to reduce computational time. A final calculation on the hexasaccharide GlcA-GlcNAc-GlcA-GlcNAc-GlcA-GlcNAc gave the same results. Two representative trajectories are shown in Figures 8 and 9. To ensure that the structures were not

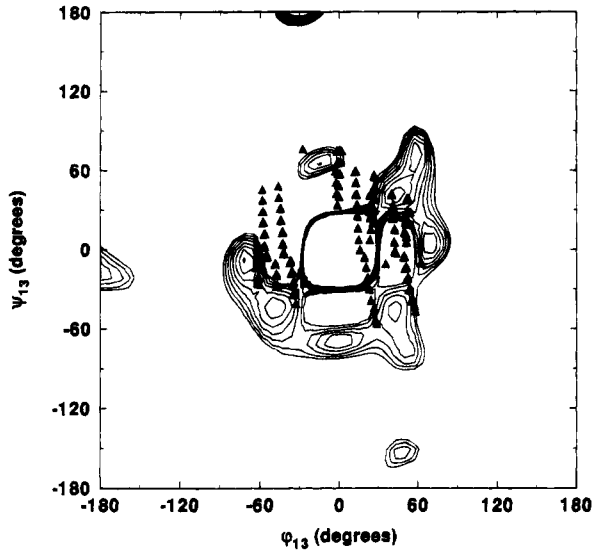


FIGURE 7: Energy contour plot for $\phi_{13}$ and $\psi_{13}$ glycosidic angles for the HA disaccharide GlcA-$\beta$(1,3)-GlcNAc. Contour lines represent a 2 kcal/mol increment in energy. $\phi_{13}$ and $\psi_{13}$ pairs for structures found to be consistent with observed NOE build-up rates are indicated with solid triangles.

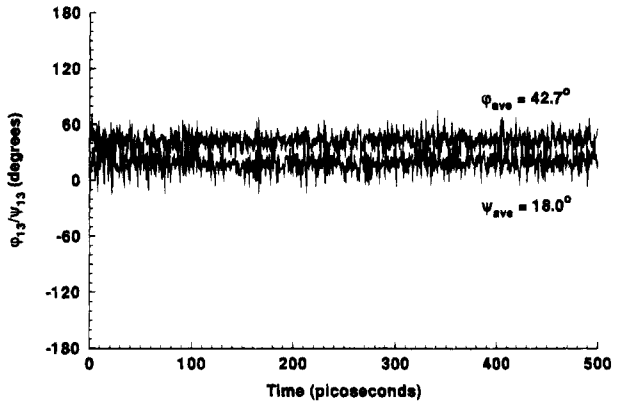


FIGURE 8: Restrained molecular dynamics trajectories for $\phi_{13}$ and $\psi_{13}$ angles of the GlcA-GlcNAc-GlcA HA trisaccharide, calculated with GB/SA solvation parameters as described in the text.

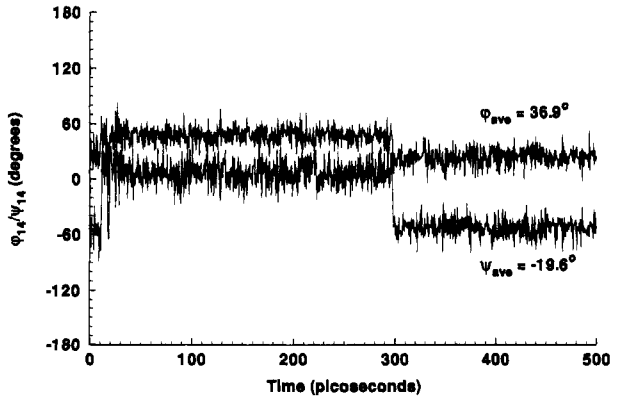


FIGURE 9: Restrained molecular dynamics trajectories for the $\phi_{14}$ and $\psi_{14}$ angles of the GlcA-GlcNAc-GlcA HA trisaccharide, calculated with GB/SA solvation parameters as described in the text.

falling into local minima and that the behavior of the trimer remained the same for all simulations, the initial values for the glycosidic dihedral angles were set to either 0° or 180°, and runs were performed at three temperatures: 300, 400, and 500 K. Standard deviations for the dihedral angle values during the course of several runs are given in Table 4. Table 5 lists the unweighted average glycosidic linkages from the molecular dynamics trajectories, plus the standard deviations for these angles during each trajectory. Table 4 represents the final optimized structure after dynamics and minimization, whereas Table 5 indicates how much the interglycosidic angles change during the dynamics runs. It can be seen that the temperature of the simulation had virtually no effect on the calculated angles.

The $\phi$ and $\psi$ values for the 1,3-linkage remained virtually constant throughout all simulations. The only exception was the early period of the 300 K simulation starting with $\phi$ = 0° and $\psi$ = 0°. This is due to an unminimized starting conformation, that is, the glycosidic angles were rotated but the structure was not optimized with these dihedral angles held constant. The minimization actually took place during the first 50 ps of the simulation. This was confirmed by monitoring the energy, which had large amplitude swings but settled down after this initial time period. Temperature had no effect, in that even performing the simulation at 500 K did not lead to additional conformations.

In contrast, the 1,4-linkage shows heightened conformational mobility. This is not apparent in the 300 K simulation starting with $\phi$ = 0°, $\psi$ = 0°. However, all of the other simulations clearly suggest the presence of two different conformations about the glycosidic linkage. The average and final $\phi$ and $\psi$ values for the 1,4-linkage confirm these observations.

To investigate the influence of the NMR-derived constraints on the calculated flexibility of the interglycosidic linkages, unrestrained molecular dynamics simulations were also performed on the HA trisaccharide. These also revealed greater conformational flexibility about the 1,4-linkage, while the 1,3-linkage remained in a single conformation. However, the weighted average distances calculated from the unrestrained trajectories were outside the experimental distances (Table 3), indicating that these simulations may not be physically relevant. In other words, the force field used leads to greater conformational flexibility for the 1,4-linkage, with or without NMR-derived constraints, although without constraints the force field does not yield distances that are consistent with the NOE data.

## DISCUSSION

The global conformation of HA is defined by the torsion angles of the glycosidic linkages and the orientation of the side groups. The $\phi$ and $\psi$ maps for the $\beta$(1,3)- and $\beta$(1,4)-linkages (Figures 7 and 5, respectively) show the range of glycosidic angles for the two linkages allowed by the NMR data, assuming a static structure for the oligosaccharide. Although these angles fall at or near the low-energy minimum in each case, the possibility of multiple conformations cannot be ruled out. The question of carbohydrate flexibility, and how to determine carbohydrate conformations taking flexibility into consideration, is currently a topic of intense debate (Bush, 1992; Tvaroska, 1992; Homans, 1993; Rutherford et al., 1993). Early NMR determinations of carbohydrate conformations were based on the assumption of a single rigid conformation in which there was no change about the glycosidic linkages with time (Bush, 1992). However, the measured NOE results from the weighted average of all conformations present, and if the molecule under study exchanges between two or more conformations,

Table 5: Unweighted Average Glycosidic Linkage $\phi$, $\psi$, and Amide Dihedral Angles from 500 ps Restrained Molecular Dynamics Trajectories[a]

| starting structure | temp (K) | $\phi_{13}$ (deg) | $\psi_{13}$ (deg) | $\phi_{14}$ (deg) | $\psi_{14}$ (deg) | amide H2−C2−N−H (deg) |
|---|---|---|---|---|---|---|
| 0° | 300 | 45 ± 9 | 18 ± 11 | 23 ± 24 | −54 ± 9 | 180 ± 13 |
| 0° | 400 | 45 ± 10 | 16 ± 14 | 48 ± 10 | 10 ± 18 | 169 ± 17 |
| 0° | 500 | 44 ± 12 | 16 ± 14 | 45 ± 14 | 2 ± 28 | 169 ± 18 |
| 180° | 300 | 44 ± 9 | 21 ± 10 | 15 ± 30 | −36 ± 30 | 189 ± 15 |
| 180° | 400 | 44 ± 10 | 21 ± 11 | 48 ± 12 | 8 ± 18 | 183 ± 17 |
| 180° | 500 | 43 ± 10 | 18 ± 11 | 37 ± 15 | −20 ± 32 | 187 ± 18 |

[a] In the first column, 0° indicates that all four glycosidic angles were at 0° for the starting structure, and 180° indicates that all four glycosidic angles were 180° in the starting structure. Standard deviations during the course of each trajectory are given.

Table 6: Dihedral Angles of $HA_4$ for Both Solution Structures and for X-ray Fiber Diffraction Structures of High MW HA Found in the Brookhaven Protein Data Bank (Abola et al., 1987; Bernstein et al., 1977)

| angle | solution structure (1) (deg)[a] | solution structure (2) (deg) | X-ray, $Na^+$ trigonal[b] (deg) | X-ray, $Na^+$ tetragonal[c] (deg) | X-ray, $Na^+$ orthorhombic (deg)[c] |
|---|---|---|---|---|---|
| $\phi_{13}$ | 46 | 46 | 54.4 | 75.3 | 68.5 |
| $\psi_{13}$ | 24 | 24 | −1.7 | −13.5 | −7.1 |
| $\phi_{14}$ | 24 | 48 | 37.4 | 40.0 | 39.8 |
| $\psi_{14}$ | −53 | 8 | −16.4 | 11.8 | 7.5 |
| amide H2−C2−N−H | −178 | −175 | −155.6 | −139.7 | −158.3 |

[a] Angles listed for the solution structures are averages over all of the structures calculated in simulated annealing runs. [b] Winter et al., 1975. [c] Guss et al., 1975.

interpretation of the NOE in terms of a single conformation will be incorrect, and the structure determined will either not exist or be only partially populated (Cummings & Carver, 1987). For peptides, fairly direct evidence for conformational flexibility has come from cases where a single conformation could not be found that met all of the NMR constraints (Kessler et al., 1988). For carbohydrates, however, there are usually too few NMR constraints, and evidence for flexibility has been taken, instead, from molecular energy calculations (Tvaroska, 1992; Cummings & Carver, 1987). These calculations have shown that multiple low-energy structures may exist for a glycosidic linkage. Furthermore, in some cases the NMR-derived conformation was not consistent with any of the calculated low-energy structures. This meant that either the NMR-derived conformation was an average conformation and the molecule was flexible, or that the force fields employed to model the molecule were inaccurate. (Of course, it is also possible that the NMR data were not accurate.)

A variety of approaches has been used in an attempt to gain information on the possible conformations of complex carbohydrates (Cumming & Carver, 1987; Bush et al., 1986; Cagas & Bush, 1990; Homans et al., 1987; Homans & Forster, 1992; Imberty et al., 1989; Rutherford et al., 1993). Recently, the approach of using NOE constraints as pseudoenergy terms in restrained molecular dynamics with simulated annealing calculations has been successfully applied to oligosaccharides (Homans & Forster, 1992; Rutherford et al., 1993). A similar approach has been applied here for conformational analysis and to assess the extent of internal motion in the HA octasaccharide. Two structures were found, with glycosidic angles listed in Table 4. The $\phi_{13}$ and $\psi_{13}$ glycosidic angles are essentially the same in both structures, while the $\phi_{14}$ and $\psi_{14}$ angles differ between the two structures, suggesting that the 1,3-linkage is relatively rigid while the 1,4-linkage is more flexible.

Simple conformational analysis of the 1,3 vs 1,4 dimer based on stereoelectronic considerations and intramolecular hydrogen-bonding contacts suggests that the $\beta$(1,4) dimer should possess a more rigid glycosidic linkage than the 1,3 dimer. This analysis assumes (1) that the exoanomeric effect, i.e., n(O)→$\sigma$*(CO) interactions (Thogerson et al., 1982) will limit the total number of conformations about a $\beta$-glycosidic linkage, (2) that solvent does not participate directly in the disaccharide secondary structure, and (3) that intramolecular hydrogen bonds to carboxylates are in the range of 1.65−1.8 Å [as shown for carboxylate groups in crystals by Gorbitz and Etter (1992)]. Given these assumptions, the $\beta$(1,4) dimer could engage in an intramolecular hydrogen bond between the NH of the acetamido moiety and the carboxylate on the adjacent GlcA ($r$ = 1.69 Å), as proposed by Guss et al. (1975) on the basis of X-ray diffraction data. This hydrogen bond would limit the mobility about the 1,4-glycosidic linkage. By contrast, the $\beta$(1,3) dimer has a closest approach between the GlcNAc NH and the adjacent carboxylate of 2.2 Å, suggesting little possibility of intramolecular hydrogen bonding, which would translate into increased conformational mobility. The results of the molecular dynamics trajectories contradict this simple, noncomputational analysis of the individual linkages and show that, in both the restrained and unrestrained cases, the 1,4-linkage has greater conformational flexibility than the 1,3-linkage.

In NMR spectra of linear carbohydrates, the repeating units overlap. Therefore, any heterogeneity in the $\phi$ and $\psi$ glycosidic angles is masked and cannot be determined without the use of selective labeling. While there is certainly some variation in the glycosidic angles along the chain, we can get an idea of the extent of the heterogeneity from the NOESY and HSQC-NOESY spectra and the molecular dynamics simulations. The HSQC-NOESY revealed a strong NOE between GlcNAc H1 and GlcA H4 and no intensity between GlcNAc H1 and GlcA H5, indicating that in none of the 1,4-linkages does the orientation of the $\phi_{14}$ and $\psi_{14}$ angles vary widely enough for GlcA H5 to be near GlcNAc H1 for any significant length of time. Similarly, for the 1,3-linkage, no NOE intensity was seen between GlcA H1 and GlcNAc H4 or H2. The molecular dynamics trajectories reveal the extent of the motional averaging across the

linkages and give an indication of the variability within the chain.

We compare the $\phi$, $\psi$, and amide group dihedral angles for our structures to those for previously published X-ray diffraction structures (Guss et al., 1975; Winter et al., 1975, 1977) of high molecular weight hyaluronan fibers (Table 6). Although the angles for the X-ray and solution structures differ, all of the $\phi$ and $\psi$ angles are between 90° and −90°. For the $\beta$(1,3)-linkage, the orientation of the rings with respect to each other (the GlcNAc ring with respect to the GlcA ring) is similar and within 6° for the solution conformations and the fiber conformations. This is not the case for the $\beta$(1,4)-linkage, where there is a greater degree of variability in the orientation of the GlcA ring with respect to the GlcNAc ring, both within families of fiber and solution structures and between them. The amide group in the solution structure is also more nearly trans than in the fiber structures. Our structure retains the general extended helical conformation of the solid state HA. If the structure with $\phi_{14} = 48°$ and $\psi_{14} = 8°$ is repeated over and over to create polymeric HA, there would be approximately 2.4 residues per turn in the helix, compared with approximately 4.4 residues per turn for the structure with $\phi_{14} = 24°$ and $\psi_{14} = -53°$ (4.6 residues/turn for the GlcNAc-GlcA unit and 4.2 residues/turn for the GlcA-GlcNAc unit), in the same range as for structures based on X-ray diffraction of fibers and films of HA (see Table 6). These values were generated by determining the degree of rotation per disaccharide and dividing this angle into 360°. The degree of rotation per disaccharide was determined by measuring the angle between H1−C1 of one residue and H1−C1 of the same residue on the next disaccharide. This simple analysis assumes that the angle the anomeric proton makes with a plane through the carbohydrate ring is constant for all rings.

In summary, we have found that although strong coupling is often ignored, it clearly can have an important effect on NOE intensity and should be taken into account. This problem is exacerbated in HA because of the nearly total overlap of several resonances. In this paper, however, we have shown that it is possible to extract the desired internuclear distances in the presence of strong coupling and extreme overlap. From these distances and molecular dynamics calculations, we determined two conformations for the HA oligosaccharide.

## ACKNOWLEDGMENT

The authors gratefully acknowledge David Brandt, Mary Cowman, James Kimura, James Rasmussen, William Westler, Wanda Sicińska, and Philip Hajduk for their helpful advice during the course of this work.

## REFERENCES

Abola, E. E., Bernstein, F. C., Bryant, S. H., Koetzle, T. F., & Weng, J. (1987) in *Crystallographic Databases—Information Content, Software Systems, Scientific Applications* (Allen, F. H., Bergerhoff, G., & Sievers, R. Eds.) pp 107−132, Data Commission of the International Union of Crystallography, Bonn.

Bax, A., & Davis, D. G. (1986) in *Advanced Magnetic Resonance Techniques in Systems of High Molecular Complexity* (Niccolai, N., & Valensin, G., Eds.) pp 21−48, Birkhaus, Basel, Switzerland.

Bax, A., & Subramanian, S. (1986) *J. Magn. Reson. 67*, 565−569.

Bernstein, F. C., Koetzle, T. F., Williams, G. J. B., Meyer, E. F., Jr., Brice, M. D., Rodgers, J. R., Kennard, O., Shimanouchi, T., & Tasumi, M. (1977) *J. Mol. Biol. 112*, 535−542.

Bertrand, P., & Delpech, B. (1985) *J. Neurochem. 45*, 434−439.

Bignami, A., Perides, G., & Rahemtulla, F. (1993) *J. Neurosci. Res. 34*, 97−106.

Braccini, I., Michon, V., Hervé du Penhoat, C., Imberty, A., & Pérez, S. (1993) *Int. J. Biol. Macromol. 15*, 52−55.

Brown, J. J. G., & Papaioannou, V. E. (1992) *Differentiation 52*, 61−68.

Bush, C. A. (1992) *Curr. Opin. Struct. Biol. 2*, 655−660.

Bush, C. A., Yan, Z.-Y., & Rao, B. N. N. (1986) *J. Am. Chem. Soc. 108*, 6168−6173.

Bystrov, V. F., Ivanov, V. T., Portnova, S. L., Balashova, T. A., & Ovchinnikov, Yu. A. (1973) *Tetrahedron 29*, 873−877.

Cagas, P., & Bush, C. A. (1990) *Biopolymers 30*, 1123−1138.

Christner, J. E., Brown, M. L., & Dziewiatkowski, D. D. (1977) *Biochem. J. 167*, 711−716.

Christner, J. E., Brown, M. L., & Dziewiatkowski, D. D. (1979) *J. Biol. Chem. 254*, 4624−4630.

Clore, G. M., & Gronenborn, A. M. (1989) *J. Magn. Reson. 84*, 398−409.

Cowman, M. K., Cozart, D., Nakanishi, K., & Balazs, E. A. (1984) *Arch. Biochem. Biophys. 230*, 203−212.

Cumming, D. A., & Carver, J. P. (1987) *Biochemistry 26*, 6664−6676.

DeMarco, A., Llinas, M., & Wüthrich, K. (1978) *Biopolymers 17*, 637−650.

Frost, S. J., Raja, R. H., & Weigel, P. H. (1990) *Biochemistry 29*, 10425−10432.

Goldstein, L. A., Zhou, D. F. H., Picker, L. J., Minty, C. N., Bargatze, R. F., Ding, J. F., & Butcher, E. C. (1989) *Cell 56*, 1063−1072.

Gorbitz, C. H., & Etter, M. C. (1992) *J. Am. Chem. Soc. 114*, 627−631.

Guss, J. M., Hukins, D. W. L., Smith, P. J. C., Winter, W. T., Arnott, S., Moorhous, R., & Rees, D. A. (1975) *J. Mol. Biol. 95*, 259−384.

Hajduk, P. J., Horita, D. A., & Lerner, L. (1993) *J. Am. Chem. Soc. 115*, 9196−9201.

Hardwick, C., Hoare, K., Owens, R., Hohn, H. P., Hook, M., Moore, D., Cripps, V., Austen, L., Nance, D. M., & Turley, E. A. (1992) *J. Cell Biol. 117*, 1343−1350.

Hascall, V. C., & Heinegard, D. (1974) *J. Biol. Chem. 249*, 4242−4249.

Hofmann, H., Schmut, O., Sterk, H., & Polzler, H. (1983) *Int. J. Biol. Macromol. 5*, 229−232.

Holmbeck, S., & Lerner, L. (1993) *Carbohydr. Res. 239*, 239−244.

Homans, S. W. (1993) *Glycobiology 2*, 551−555.

Homans, S. W., & Forster, M. (1992) *Glycobiology 2*, 143−151.

Homans, S. W., Pastore, A., Dwek, R. A., & Rademacher, T. W. (1987) *Biochemistry 26*, 6649−6655.

Hricovíni, M., Shah, R. N., & Carver, J. P. (1992) *Biochemistry 31*, 10018−10023.

Imberty, A., Tran, V., & Pérez, S. (1989) *J. Comput. Chem. 11*, 205−216.

Keeler, J., Neuhaus, D., & Williamson, M. (1987) *J. Magn. Reson. 73*, 45−68.

Keepers, J. W., & James, T. L. (1984) *J. Magn. Reson. 57*, 104−426.

Kessler, H., Oshkinat, H., Griesinger, C., & Bermel, W. (1986) *J. Magn. Reson. 70*, 106−133.

Kessler, H., Griesinger, C., Lautz, J., Muller, A., van Gunsteren, W. F., & Berendsen, H. J. (1988) *J. Am. Chem. Soc. 110*, 3393−3396.
Knudson, C. B. (1993) *J. Cell Biol. 120*, 825−834.
Laurent, T. C. (1987) *Acta Otolaryngol. Suppl. 442*, 7−24.
Livant, P., Rodén, L., & Rama Krishna, N. (1992) *Carbohydr. Res. 237*, 271−281.
Macura, S., & Ernst, R. R. (1980) *Mol. Phys. 41*, 95−117.
Marion, D., & Bax, A. (1989) *J. Magn. Reson. 83*, 205−211.
Mohamadi, F., Richards, N. G. J., Guida, W. C., Liskamp, R., Lipton, M., Caufield, C., Chang, G., Hendrickson, T., & Still, W. C. (1990) *J. Comput. Chem. 11*, 440−467.
Peng, J. W., & Wagner, G. (1992) *J. Magn. Reson. 98*, 308−332.
Piantini, U., Sørenson, O. W., & Ernst, R. R. (1982) *J. Am. Chem. Soc. 104*, 6800−6801.
Plateau, P., & Guéron, M. (1982) *J. Am. Chem. Soc. 104*, 7310−7311.
Poppe, L., & van Halbeek, H. (1992) *J. Am. Chem. Soc. 114*, 1092−1094.
Ramachandran, G. N., Chandrasekaran, R., & Kopple, K. D. (1971) *Biopolymers 10*, 2113−2131.
Ramsden, L., & Rider, C. C. (1992) *Eur. J. Immunol. 22*, 3027−3031.
Rutherford, T. J., Partridge, J., Weller, C. T., & Homans, S. W. (1993) *Biochemistry 32*, 12715−12724.
Scott, J. E., Heatley, F., & Hull, W. E. (1984) *Biochem. J. 220*, 197−205.
Sicińska, W., Adams, B., & Lerner, L. (1993) *Carbohydr. Res. 242*, 29−51.
Siczkowski, M., Amos, T. A. S., & Gordon, M. Y. (1993) *Exp. Hematol. 21*, 126−130.
Specks, U., Mayer, U., Nischt, R., Spissinger, T., Mann, K., Timpl, R., Engel, J., & Chu, M.-L. (1992) *EMBO J. 11*, 4281−4290.
Stamenkovic, I., Amiot, M., Pesando, J. M., & Seed, B. (1989) *Cell 56*, 1057−1062.
Still, W. C., Tempczyk, A., Hawley, R. C., & Hendrickson, T. (1990) *J. Am. Chem. Soc. 112*, 6127−6129.
Summers, M. F., Marzilli, L. G., & Bax, A. (1986) *J. Am. Chem. Soc. 108*, 4285−4294.
Thogersen, H., Lemieux, R. U., Bock, K., & Meyer, B. (1982) *Can. J. Chem. 60*, 44−57.
Toffanin, R., Kvam, B. J., Flaibani, A., Atzori, M., Biviano, F., & Paoletti, S. (1993) *Carbohydr. Res. 245*, 113−128.
Toole, B. P. (1990) *Curr. Opin. Cell Biol. 2*, 839−844.
Toole, B. P. (1991) in *Cell Biology of the Extracellular Matrix* (Hay, E. H., Ed.) pp 305−341, Plenum Press, New York.
Toole, B. P., Jackson, G., & Gross, J. (1972) *Proc. Natl. Acad. Sci. U.S.A. 69*, 1384−1386.
Tvaroska, I. (1992) *Curr. Opin. Struct. Biol. 2*, 661−665.
Underhill, C. (1992) *J. Cell Sci. 103*, 293−298.
Winter, W. T., & Arnott, S. (1977) *J. Mol. Biol. 117*, 761−784.
Winter, W. T., Smith, P. J. C., & Arnott, S. (1975) *J. Mol. Biol. 99*, 219−235.
Zimmerman, D. R., & Ruoslahti, E. (1989) *EMBO J. 8*, 2975−2981.